Microstructure characterization of CVI-densified carbon/carbon composites with various fiber distributions

S. Dietrich, J.-M. Gebert, G. Stasiuk, A. Wanner, Kay A. Weidenmann, O. Deutschmann, I. Tsukrov, R. Piat

Angaben zur Veröffentlichung / Publication details:

Dietrich, S., J.-M. Gebert, G. Stasiuk, A. Wanner, Kay A. Weidenmann, O. Deutschmann, I. Tsukrov, and R. Piat. 2012. "Microstructure characterization of CVI-densified carbon/carbon composites with various fiber distributions." *Composites Science and Technology* 72 (15): 1892–1900. https://doi.org/10.1016/j.compscitech.2012.08.009.

Microstructure characterization of CVI-densified carbon/carbon composites with various fiber distributions

S. Dietrich [a], J.-M. Gebert [a], G. Stasiuk [b], A. Wanner [a], K.A. Weidenmann [a], O. Deutschmann [c], I. Tsukrov [d], R. Piat [b,c,*]

[a] Institut für Angewandte Materialien-Werkstoffkunde (IAM-WK), Karlsruher Institut für Technologie (KIT), Kaiserstr. 12, 76131 Karlsruhe, Germany
[b] Institut für Technische Mechanik, Karlsruher Institut für Technologie, Kaiserstr. 12, 76131 Karlsruhe, Germany
[c] Institut für Technische Chemie und Polymerchemie, Karlsruher Institut für Technologie, Engesserstr. 18, 76131 Karlsruhe, Germany
[d] University of New Hampshire, Durham, NH 03824, USA

1. Introduction

Carbon/carbon composites (C/C) are materials which combine exceptional strength and stiffness (also by high temperatures about 2000 °C) with light weight, excellent refractory and corrosion properties, making them the material of choice for severe-environment applications, such as atmospheric reentry, solid rocket motor exhaust, and disk brakes in high performance military and commercial aircraft, high speed trains and racing cars. According to surveys of the C/C business prospectus, "there are a whole host of applications ideally suited to the properties of C/C, provided the price is lowered as a result of more efficient fabrication" [1,2]. The mechanical behavior of these materials with complicated hierarchical structures is strongly influenced by the distribution and shape of their microconstituents: fibers, pores and pyrolytic carbon (PyC) coating. This fact is especially exciting for the reason that these parameters can be controlled by the manufacturing process and production of the materials with orientation dependent stiffness or strength is possible.

One of the often used methods for production of the C/Cs is chemical vapor infiltration (CVI) of carbon fiber preforms. It presents an example when a complex hierarchical microstructure is adjustable by manufacturing conditions [3,4]. In C/C, carbon fibers are embedded in a matrix of PyC which has a cylindrically layered structure [5] dependent on the deposition parameters. By changing the CVI parameters, e.g. pressure, temperature, precursor or residence time, it is possible to obtain different textures of the PyC coating [3,4], and thus change the mechanical properties of the coating [6–8].

The main microstructural components of C/Cs are fibers, pores and PyC coating which deposits around carbon fibers during CVI process. The elastic and thermal properties of carbon fibers are transversally isotropic with sharp contrast between the longitudinal and transverse directions (e.g. for P-100-H carbon fibers, E_{long} = 770 GPa and E_{trans} = 7.1 GPa [9]). For this reason, deviation of fibers from their desired orientation might cause significant changes in the composite material response.

Experimental studies of the material properties of C/Cs on a macro scale for different fiber architectures, different porosities were reported in [10], and the influence of void fraction on the flexural strength and modulus was studied. An analytical modeling

* Corresponding author.
E-mail address: romana.piat@kit.edu (R. Piat).

approach for predicting the stiffness of 3D orthotropic composites was developed in [11]. Hatta and his group performed a comprehensive experimental study on 2D and 3D composites [12–15] to analyze their strength in tension, shear and compression tests. Casal et al. [16] addressed the influence of porosity on the shear strength of the composite. All these studies show that fiber orientations and porosity have crucial influence on the mechanical and thermal [17] properties of these composites.

An approach to estimation of fiber orientations in the short fibers composites using 2D image analysis was given by Mlekusch [18]. In that work, the fiber orientation distribution function was shown as a density on the unit sphere. The fiber orientation measurements based on the image analysis were presented in the form of polar graphs by Blanc et al. [19].

Development of the X-ray micro-tomography (μCT) has provided new possibilities for effective quantification of the fiber and pore distributions. This technique was utilized by Bernasconi et al. [20] for the local anisotropy analysis of injection molded short-fiber reinforced polymer composites. They applied the mean intercept length (MIL) method to construct the fabric tensor which characterizes the fiber distribution. In Cosmi et al. [21], a combination of MIL with the phase contrast (PHC) imaging techniques was utilized for analysis of a short carbon fiber reinforced polyamide. 3D-quantification of the distribution of continuous fibers in unidirectionally reinforced composites was given by Requena et al. [22]. In the present paper, the μCT technique is utilized to obtain data on various fiber preforms; this data is then processed with a self-written C++ code to produce the probability distribution functions of fiber orientations.

Another microconstituent that has crucial influence on thermoelastic properties of C/C composites is porosity. In our previous studies of unidirectional (UD) and infiltrated felt composites [23–25] the analysis of pore shapes was based on the micrographs of the cross-sections of the samples. The 2D studies of the porosity were assumed to be possible for those two types of materials because in the UD composite the pores are long in the longitudinal direction and the plane strain assumption can be used, while in the infiltrated felt the fiber distribution is random and the pores can be treated as having the same shape in all directions.

The 2D-micrograph based estimates can be improved for complex pore shapes by utilizing the 3D information on material microstructure obtained by μCT technique. In publications by Gebert et al. [26], and more recently Drach et al. [27], our first steps in the development of a pore identification technique and its application for carbon/carbon composites were reported. In this paper, we provide advancement in the technique which includes development of the probability distribution functions for pores present in variously reinforced C/C composites.

This paper is organized as follows. Section 2 discusses the C/C manufacturing process and the main factors defining microstructure of the composites. Data on the dependence of material density and PyC coating thickness on infiltration time is also provided. Section 3 presents the fiber orientation extraction procedure. Section 4 deals with characterization of the local PyC coating thickness in the composites. Section 5 is devoted to classification and analysis of pores in the material.

2. Manufacturing parameters influencing microstructure

CVI is one of the commonly used methods for fabrication of C/C composites with PyC. During this process, the carbon fiber preform is infiltrated by hydrocarbon gas in a hermetically closed high temperature reactor, and PyC matrix deposits on fiber surfaces filling the space between fibers. The materials studied in this paper were produced by isothermal, isobaric CVI; the process was performed at a constant temperature of 1095°. Two materials were manufactured by infiltrating preforms made of long continuous fibers. The first material: carbon fiber felt with 7.1% volume fraction of the fibers was infiltrated by pressure of 10 kPa, residence time of 0.1s (infiltration time 25, 45 and 120 h). The second material: 2D carbon fibers preform with 22.5% volume fraction of fibers was infiltrated by pressure of 20 kPa, residence time of 0.1 s (infiltration time 20, 60 and 120 h). In both materials, the resulting PyC matrix has a layered structure with each layer exhibiting different texture [28,29]. The texture of the matrix and thickness of the layers depend on the production parameters such as pressure, type of the precursor gas, and temperature in the reactor [30]. The infiltration of the composites was carried out at the Institute for Chemical Technology of the Karlsruhe Institute of Technology. Details of the infiltration procedure are provided in [30].

2.1. Architecture of the fiber preform

The main factors influencing the microstructural architecture of C/Cs are the infiltration time and the orientation of fibers in a preform.

Optical microscopy images of the typical composite microstructure are presented in Fig. 1. It is possible to obtain different C/C materials depending on the preform topology: from unidirectional (UD) orientation of the fibers (all fibers are oriented in one direction) to an infiltrated felt with random distribution of fibers. All these materials have certain porosity, the distribution and shapes of pores are dependent on the preform structure, and the volume fraction of the porosity can be controlled through the infiltration time. The microscale structural unit of all these composites is a fiber with pyrolytic carbon coating.

In this paper, two preform architectures with long continuous carbon fibers were considered. The first one is the so-called "2D preform" produced by Surface Transforms (Ellesmere Port, UK) with fiber diameter about 10 μm [29]. The second one is the random felt produced by Conradty (Nürnberg, Germany) with fiber diameter about 10 μm [31]. Both preforms consist of HT carbon fibers (Panox®, SGL Carbon) with E = 190 GPa in fiber direction and density of 1.72 g/cm^3 [32].

The "2D preform" based material has a laminated structure with 0°/0°/90°/90° unidirectional layers having thickness l_u = 1.05 mm separated by thin layers of felt material (l_f = 0.2 mm between UD layers of the same orientation and l_f = 0.4 mm between UD layers perpendicular to each other) [29], as presented in Fig. 1. The stack of layers is needled by a small number of fibers in the direction perpendicular to the laminate plane (i.e. direction 3 in Fig. 1b) to hold it together before and during infiltration. The micrograph showing the local microstructure of layers having a preferred orientation and separated by a felt layer, as well as the micrograph of the analyzed part of the laminated microstructure is presented in Fig. 1a.

Analysis of the felt preform microstructure (Fig. 1c) shows that it contains fibers that are randomly oriented in the 1–2 plane, as well as some fiber bundles with preferred orientation in the third direction. For this reason it is expected that the material based on this preform will be transversally isotropic.

2.1.1. Influence of the infiltration time on the microstructure, density, porosity of the material and on the texture of the PyC coating

The thickness of the PyC coating around fibers is dependent on infiltration time and fiber packing in the composite. Optical microscopy images of laminated ("2D preform") and random felt composites for different infiltration time are presented in Fig. 1d and e. For the infiltration time of 20–25 h, the PyC coating is very thin; however, its thickness increases with infiltration time for both composites. It is also recognizable that the fiber packing in

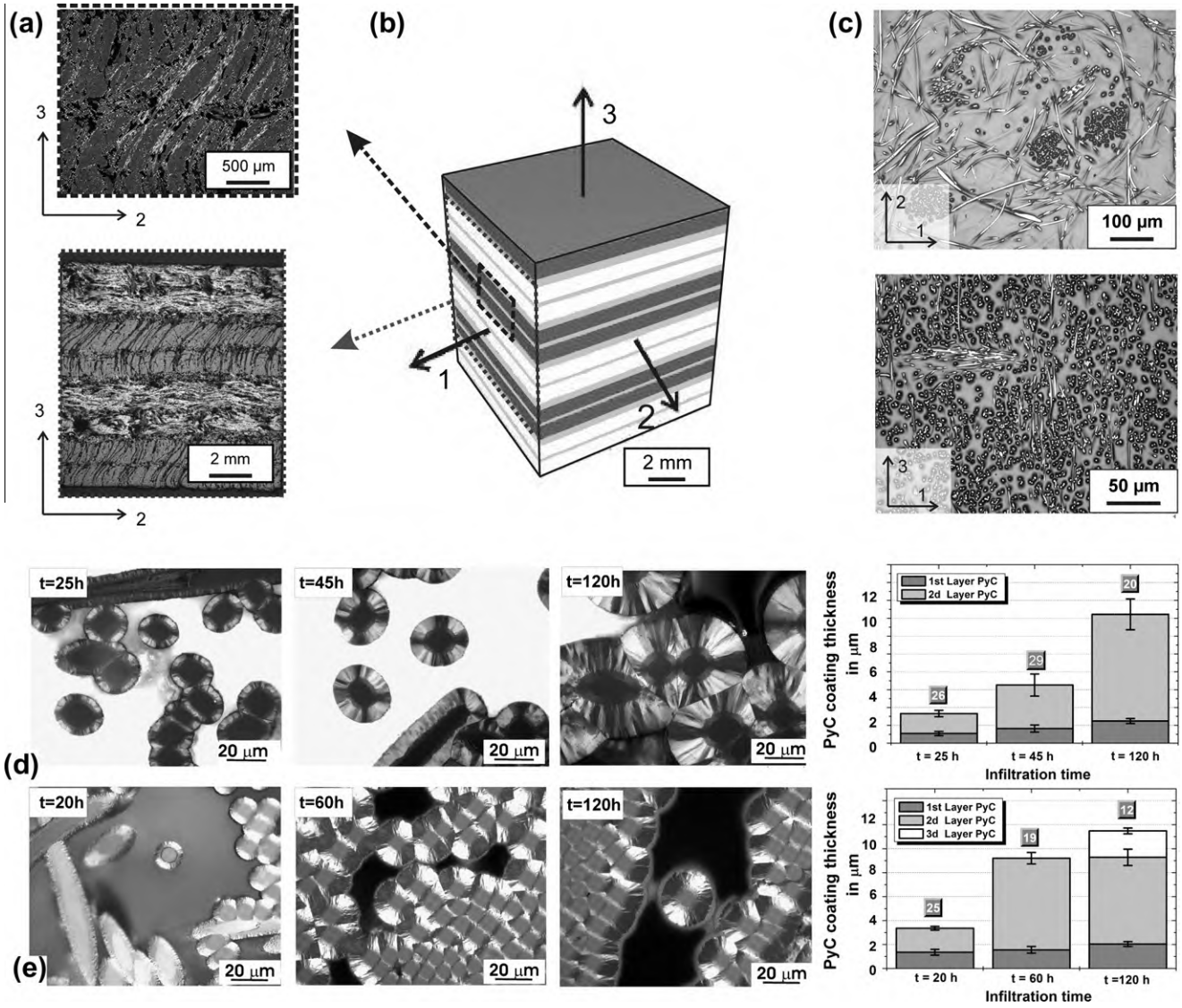

Fig. 1. Typical microstructure of the material based on 2D preform: (a) local image of two UD layers separated by felt and material consisting of eight UD layers separated by felt; (b) schematic representation of the entire 2D preform. Dark gray and white colors represent differently oriented UD layers, felt is shown by light gray; (c) typical microstructure of the felt preform in two perpendicular directions; light microscopic images [32] of the local material microstructure and thickness of the coating for different infiltration time of the (d) felt for 25 h, 45 h and 120 h corresponding and (e) 2D preform for 20 h; 60 h and 120 h.

a composite influences the thickness of fiber coatings. Fig. 1d (the right part) shows that in the regions with very dense fiber packing, the PyC coating is not as thick as in the porous regions. Another observation based on the studies provided in [33] is that it is impossible to completely eliminate residual porosity neither with the longer infiltration time nor with repetitive successive infiltration.

The thickness of the deposited PyC for the studied material was determined from 2D images similar to the ones shown in Fig. 1a. Fibers that are oriented perpendicular to the cross section were fitted by two circles, one fitting the fiber and the other one including the fiber plus the deposited PyC. The difference in the radii of the circles equals to the thickness of the deposited PyC layer. The values of the thickness for random felt and 2D preform composites are shown in Fig. 1d and e. The thickness of the coating is given in μm, and the number in the box corresponds to the number of the measured fibers.

As can be seen in Fig. 1c and d, the PyC coating in both composites consists of the layers with different texture [29]. Studies of the correlation between the infiltration conditions and the resulting PyC matrix for both preforms are reported in Zhang and Hüttinger [34,35]. The infiltration conditions of the isothermal and isobaric CVI process were chosen in such a way that the resulting PyC matrix is mostly high textured (see Table 1). Texture degree can be characterized by the orientation angle as discussed in [28]. The estimated values of OA for both composites are provided in Table 1 and were taken for fibers which were in the central part of the infiltrated sample. They show that after 120 h of infiltration, the PyC coating of the 2D preform consists of three layers. The first layer is very thin and low textured (LT), the second is thick and high textured (HT). The third layer, observed for 120 h of infiltration time, shows no optical anisotropy. At the same time, the infiltrated felt exhibits only two PyC layers. The first one is LT and the second is HT, see Table 1.

Two different methods were utilized for calculation of density of the samples:

- Calculation of density from the mass and geometry of the specimens.
- Calculation of density using the Archimedes principle.

Table 1
Textures of the PyC for felt and 2D preform specimens.

Preform type and infiltration time (in h)		Number of studied fibers	Texture of the first layer (in OA)	Texture of the second layer (in OA)	Texture of the third layer (in OA)
Felt	25	10	8.3	18.8	–
	45	10	7.7	19.7	–
	120	10	7.9	21.5	–
2D Preform	20	5	Too thin for measurement	10.6	–
	60	5	Too thin for measurement	15.1	–
	120	5	Too thin for measurement	14.4	Isotropic

The dimensions of the specimens were measured with a TESA μHite height gage from Swiss Instruments with a resolution of 1 μm for the samples with infiltration times of 60–120 h. The dimensions of the very porous samples with an infiltration time of 20 h were measured with a micrometer screw to omit any possible penetration of the tip into the specimen (resolution of 10 μm). The weights of the samples were measured with a balance from Mettler (AE240) with a resolution of 0.01 mg. The determined densities are listed in Table 2. The densities determined via Archimedes principle deviate 1–6% from the densities obtained using the mass and geometry. This error lies within the bounds of the respective standard deviation.

Another important feature is the porosity (volume fraction of pores). In our studies, two methods were utilized for porosity measurements. The first one is the standard water impregnation method to measure the open porosity. However, the metallographic images of the specimens show that some pores are closed inside of the material so they are not identifiable using the water impregnation method. For this reason, the second method based on the digital image analysis of section micrographs was also utilized. The porosity obtained using both methods is presented in Table 2. It can be seen that in most cases the image based estimates provide higher values of porosity.

3. Characterization of the fiber distribution

The three dimensional spatial distributions of fibers in the composite were characterized by performing the microcomputed tomography (μCT) studies on non-infiltrated carbon-fiber preforms. This was motivated by the fact that the contrast in density between fibers and PyC is not sufficient to reliably separate them by contrast-based μCT. However, recent scans using synchrotron sources allow for distinguishing all three image components [32,36]. The distribution of fibers does not change during CVI. Thus, the analysis of fibers in the preform prior to infiltration provides reliable information on their distribution in the manufactured composite.

A cylindrical specimen of 6 mm diameter was cut from the preform material by water cutting and scanned using a Skyscan 1072 μCT system. The scanning geometry allowed for a voxel size of 1.83 μm and an image volume size of $1536 \times 702 \times 704$ voxel. As can be seen in Fig. 2a, the organization of the fibers can be divided into two different regions. In the felt regions the orientation of the fibers in the 1–2 planes is random and more densely packed in comparison to the UD regions. Therefore the projected average gray-value of the image slices can be used as a measure for the region boundaries (see Fig. 2). The stacks of layers is held together by pinning fiber rovings to prevent the layers from moving during processing.

Insight into the fiber orientation distribution is achieved through a set of basic image processing steps. First, the image is filtered using an anisotropic diffusion filtering step [37] to enhance the difference of the tubular fibers in contrast to the unfiltered background (see Fig. 2). Application of this pre-processing step allows for an easier segmentation of the fibers as a foreground from the empty background. Its advantage lies in the distinction of blob- or plate-like features which arise from the artifacts or image noise of the imaging system.

Furthermore, in the densely packed fiber bundles or crossings of fibers, the separation of different fibers can be blurred due to the resolution limit of the CT-system. Therefore, the contrast enhancement of the pre-processing step is essential for a proper and distinct segmentation. The segmentation procedure is then conducted using a global threshold determined by Otsu's method [38] while the stability of the segmentation is barely influenced by smaller variations of the threshold value. To avoid over- or underestimation of the fibers boundaries in the binary image the parameters of the diffusion filter from [39] have been manually adjusted to reach an optimal result for the segmentation compared to the visual inspection of each gray value image.

After segmentation, the binary image is used as an input for a sequential anisotropic Gaussian filtering procedure [40] which is employed to determine the local orientation of the fiber as well as an orientation average of the fiber in form of an fiber orientation tensor (see [41]). In this approach, the image is cyclically rotated and filtered with the anisotropic ellipsoidal Gauss filter in order to identify the local orientation of each voxel including its surrounding region of interest (ROI) as determined by the filter size from the filter response connected to the current rotation angles (see Fig. 2c). The upper hemisphere was divided into 100 sampled directions with equal area for each direction. The partition procedure was performed according to [42]. The chosen number of the sampled directions is a compromise between the computation time and orientation precision. In this way a reasonable computation time and accuracy can be achieved. For example, the computation time needed for processing of the image presented in Fig. 3a was about 4 h on a Xeon Quad Core platform with 24 GB RAM.

As can be seen in Fig. 3a and b, the fiber orientation has been color-coded using the orientation of each voxel obtained by the maximum filter response. This allows for creating a 3D histogram on the sphere where the fiber fraction is plotted as intensity. Such a presentation clearly outlines the anisotropy of the material (see Fig. 3c–e).

Evaluation of the single layers shows that fiber bundles are oriented either along the 1-axis or the 2-axis. Based on the studies presented in [32], the volume fraction of the fibers in UD and felt layers is calculated to be 10% and 23%, respectively. To further analyze the preferred orientation of carbon fibers, each voxel direction corresponding to a fiber was projected onto one of the three axes of the coordinate system (see Fig. 3) reducing the data to only three parameters describing the average fiber distribution. The results of measurements show that a nearly constant amount of 30% of the fibers is oriented preferentially parallel to the 3-axis, while 60% of the fibers are oriented parallel to the direction of reinforcement (1- or 2-axes, depending on the layer), and the remaining 10% are oriented perpendicularly to the above axes.

Table 2
C/C-2D preforms and infiltrated felt: estimation of the density from mass and geometry (ρ_1) and from water impregnation Archimedes' buoyancy principle (ρ_2). The column σ/ρ_2 equals the standard deviation of all corresponding measurements divided by the mean value of the density; estimation of the porosity: the column σ/p equals the standard deviation of all corresponding measurements divided by the mean value of the porosity. Last column presents recalculated values from analysis of felt and UD images (ratio felt to UD is 2/7) for porosity of infiltrated 2D preform.

Infiltration time (h)	Number of measured specimens	Density measured from the mass and geometry		Density measured through water impregnation		Porosity measured through water impregnation		Porosity measured through image analysis				
								Felt images		UD images		All images
		ρ_1 (g/cm^3)	σ/ρ_1 (%)	ρ_2 (g/cm^3)	σ/ρ_2 (%)	p (%)	σ/p (%)	p (%)	σ/p (%)	p (%)	σ/p (%)	p (%)
Infiltrated felt												
25	15	0.34	5	0.37	5	80.1	1	86.5	5	–	–	–
45	15	0.62	6	0.68	6	65.5	3	65.2	6	–	–	–
120	15	1.36	7	1.47	5	28.2	14	28.7	15	–	–	–
Infiltrated 2D preform												
20	15	1.05	3.0	1.11	2.5	41.5	5	68.1	11	31.3	15	39.5
60	15	1.65	3.2	1.67	2.7	14.6	23	33.9	25	14.8	23	19.0
120	15	1.73	1.3	1.78	1.1	8.1	25	25.7	27	9.5	33	13.1

4. Characterization of the local coating thickness in C/C composites

Typical images of C/C microstructure (Fig. 1) show that the thickness of PyC coating in the composite varies significantly, and depends on the infiltration time and distances between fibers. After 40 h infiltration time, fibers in the packed bundles are completely infiltrated [35], and during further infiltration only the fibers at larger distances from each other – we will call them "single fibers" – experience growth of thicker PyC coating. The longitudinal elastic modulus of carbon fibers [43] is very high in comparison to the elastic modulus of PyC coating [44]. The difference in the properties in transverse direction is not so large, but for calculation of the elastic properties it is important to know the exact local volume fractions of the PyC and fibers in different parts of the composite.

Materials with 2D preform consist of the fibers that are mostly arranged in bundles [35] and some single fibers. We performed statistical studies to analyze relative amounts of fibers and PyC in the bundles and single fibers. The images for analysis are assumed to be in the plane perpendicular to the bundles. In these images, using a self-written MATLAB routine, we recognize fibers and separate them into the fibers in bundles and single fibers. The PyC coating deposition on the fibers is then simulated to provide estimates of the distribution of PyC in the bundles and around single fibers. This simulation reproduces the continuous growth of

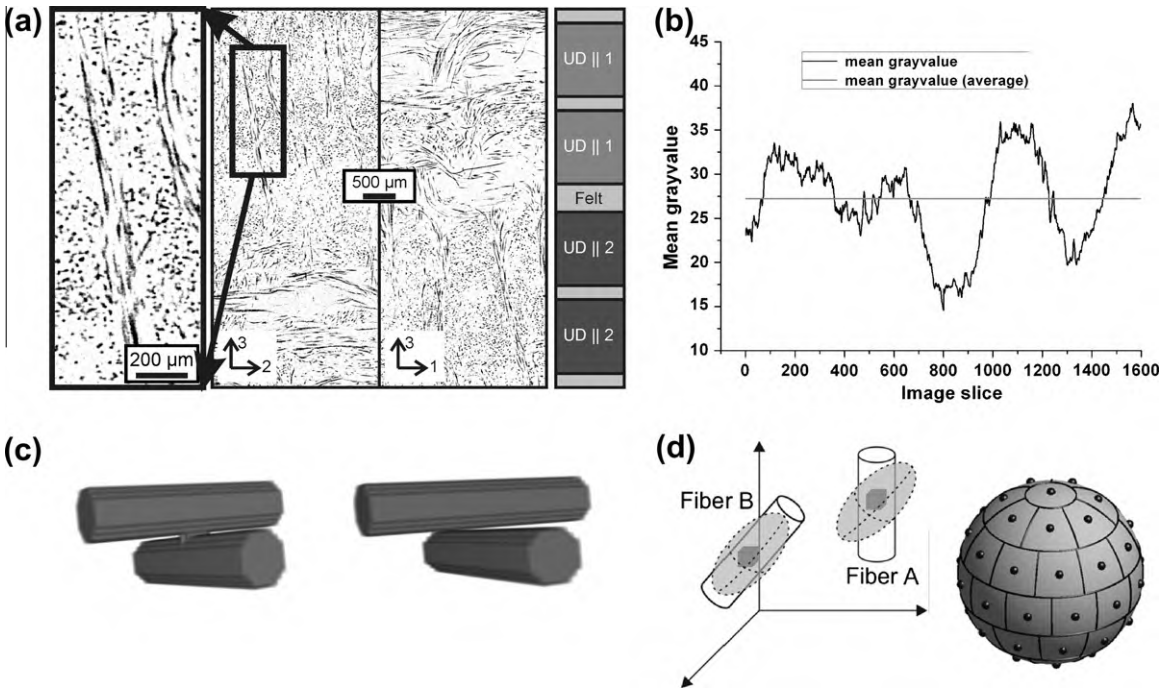

Fig. 2. (a) Orthogonal sections of µCT image of the non-infiltrated preform indicating UD and felt regions along the 3rd-direction; partition of different layers in the preform based on the mean gray value of the image slice and the entire image average; (b) areas with high gray value above the volume mean correspond to UD layers due to less fibers lying in the slice plane, regions having lower mean gray values can be related to felt layers; fiber distribution analysis; (c) test image for the anisotropic diffusion filter applied to erode the bridging between fibers after thresholding [37–39] and (d) anisotropic Gauss filtering according to the maximum filter response (fiber B, maximum overlap between filter and fiber) and reduced filter response (fiber A) for a single orientation of the probing filter: partition of the sphere for equal area sampling of the orientation histogram [42].

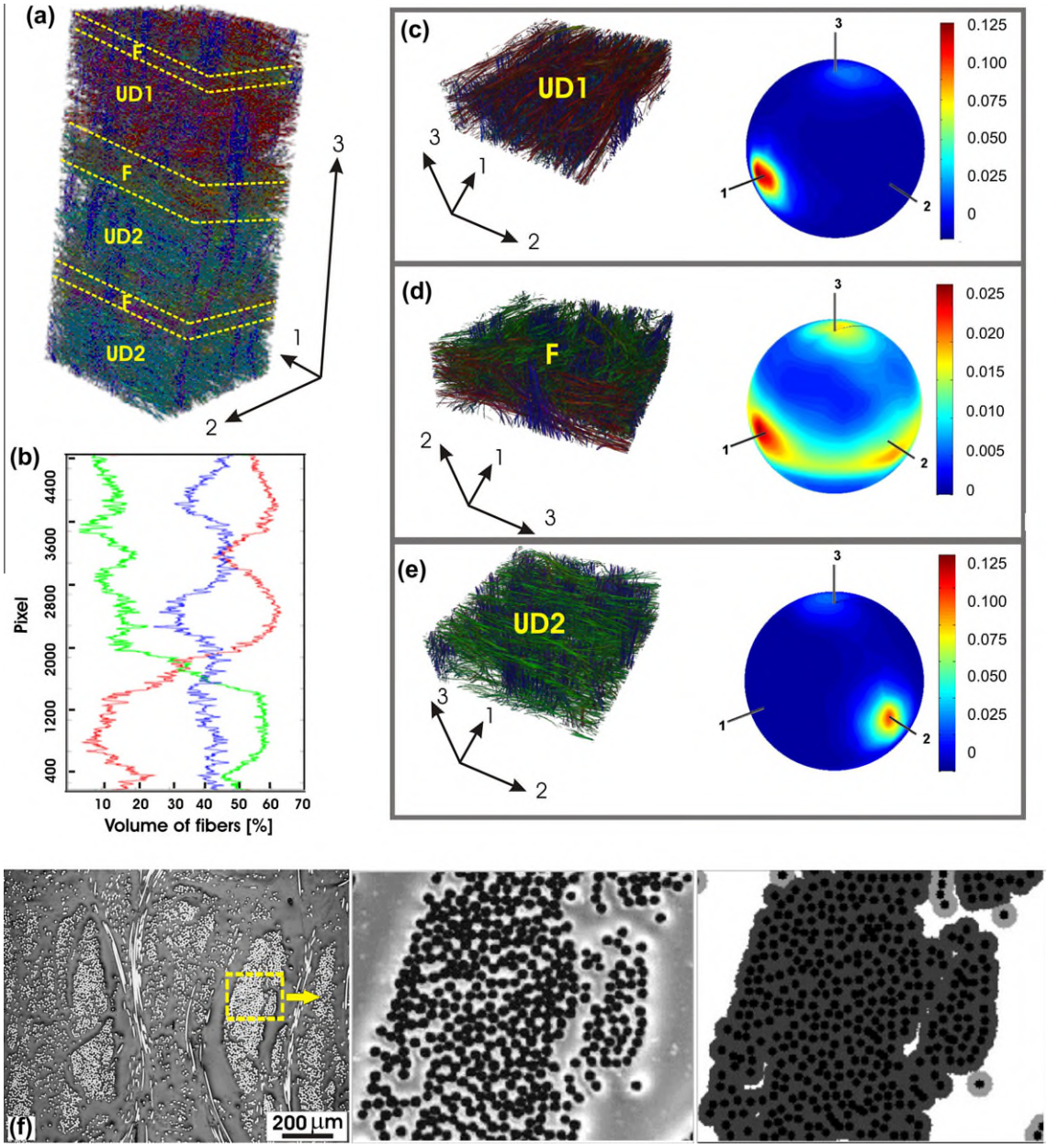

Fig. 3. (a) Color coded orientation image with 100 different rotations around the unit sphere showing two differently oriented UD-layers (UD1, UD2) with three separating felt (F) layers; (b) projection of the direction onto the sample coordinate system reveals the felt layers from the minima and maxima of the relative fiber amount; (c and e) near uniaxial fiber distribution in the UD layers (UD1, UD2) with only few *z*-pinning fibers and corresponding distribution functions; (d) orthotropic fiber distribution in the felt layer indicated by a near planar distribution of fibers in the *x*–*y*-direction plus additional pinning fibers in the *z*-direction and corresponding distribution function; (f) procedure of the fibers recognition: original image; inverted image; fibers coated by PyC using growth algorithm (light gray is PyC on single fibers, dark gray is PyC on fibers in bundles).

the coating perpendicular to the fibers axes, as in the CVI process, but takes into account only the geometric changes of the microstructure. This process take place till PyC deposits on the neighboring fibers touch each other, and predefined maximal thickness of the PyC coating of the single fibers or volume fraction of PyC is reached. The details of the procedure are described in the text below.

Using 2D microstructure images (see Fig. 3f), we recognize fibers that are perpendicular to the plane of image. Since fibers are cylindrical, they are recognized as circles. The images should be converted into black and white in order to apply recognition procedure that determines the location of the centers and mean radii of round objects (using MATLAB function of separating objects and applying the relation between the perimeter and area for circle ($4\pi S/P^2 = 1$)). Fibers touching each other cannot be recognized as round objects by this method. They have to be recognized with the mask of round object with radius equal to the mean radius of fibers recognized in the previous step. Then, the manual separation of the remaining unrecognized fibers and exclusion of not properly recognized fibers (about 0–5% of all fibers depending on the quality of the image) is performed. Having the information on location and size of fibers, we separate bundles and single fibers by solving the connectivity problem for the incidence matrix. Elements of this matrix are equal to zero if the distance between the correspondent fibers exceeds 4–6 mean radii. The groups of less than 10 connected fibers are not assumed to be bundles.

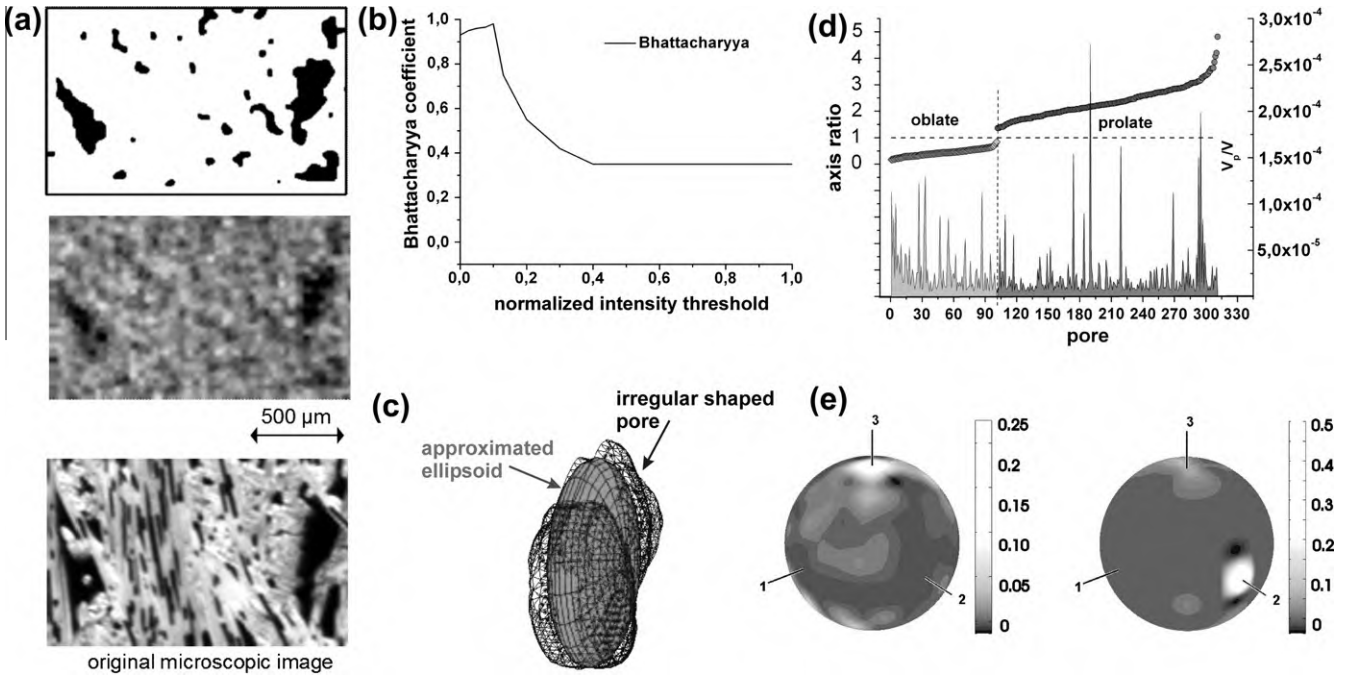

Fig. 4. (a) CT image processed using a connected component region growing algorithm; original gray value CT image with pores, optical microscopy image; (b) comparison of two registered sections from microscopic and CT data sets (top and bottom in a) using the Bhattacharyya coefficient as adequate measure for the image signal match; (c) approximation of the irregularly shaped pore by a principal component analysis fitted ellipsoid; (d) half-axis ratios and volume fraction of the observed pores; (e) orientation distributions of oblate and prolate pores in a UD layer.

The growing procedure is performed on a separate image, where the recognized fibers are showed as black circles. The PyC as circles of increasing radii are drawn around fibers: dark gray circles are for PyC around fibers in bundles and light gray around single fibers. This presentation allows us to calculate the relative amounts of the PyC in the bundles and around single fibers according to the areas of dark and light gray. The ratio between PyC around fibers in bundles and PyC around single fibers was calculated as ratio of pixels of dark and light gray colors.

The described procedure provides the volume fraction of PyC in the coating of the fibers in bundles and single fibers. Microstructure in Fig. 3f was numerically analyzed using proposed procedure and it was obtained, that 96% of all fibers are in bundles and only 4% are single fibers. In bundles the volume of the PyC coating is about 70% and in single fibers about 88%.

5. Studies of the porosity and pores approximations

5.1. Pore identification and classification of the typical pores in the C/C composite

In this section, we discuss distribution of pores in the considered materials based on the µCT data and the available optical microscopy images. One of the challenges is to extract the pore geometries from the µCT images with acceptable accuracy. To preserve the pore shapes without introducing any deviations due to image artifacts or image blurring, the segmentation procedure has been developed. It is based on the comparison of µCT and optical microscopy images. An evaluation of the applicability of different segmentation algorithms has shown that the most appropriate methods are an automatically seeded region-growing approach and a 3D geodesic active contour algorithm [45].

For the seeded region-growing segmentation to give the most accurate separation between the pores and the matrix, we compared the segmented images from the CT measurements (Fig. 4a on the top) with the processed optical microscopy (OM) 2D images of the same region (Fig 4a bottom). The µCT data (Fig. 4a in the middle) was processed with the set of parameters adjusted to produce the same porosity and pore shapes as in the OM 2D images, for which the boundary between the pores and the matrix is well defined. The µCT data processing parameters included the threshold values for the seed points and the connected components [45].

As a measure of the similarity between the images of different threshold parameter sets, the Bhattacharyya coefficient (or distance) [46,47] was used. Its dependence on the normalized intensity threshold is shown in Fig. 4b. The maximum value corresponds to the optimal µCT segmentation under the restriction of equal porosity in CT and OM images. Note that even though this algorithm minimizes the discrepancy between the images, the representation of pores shapes is still not identical.

In the next segmentation step, the binary image was labeled to enumerate different pores. The resulting image was processed with a label analyzer filter to extract statistical information on pores for various regions of the composites. The pore shapes extracted from the labeled pores were approximated by ellipsoids utilizing the principal component analysis as described in our previous publication [27,48]. Fig. 4c provides an example of the irregular pore and the corresponding approximating ellipsoid.

Fig. 4d and e presents information on pore distribution in the unidirectional part of laminated composite shown in Fig. 3e. The histograms for the pore volumes and half-axis ratios are shown in Fig. 4d. It is seen that two types of pores, oblate and prolate, can be identified in that layer. Distributions of their orientations are shown in Fig. 4e and d, correspondingly. The prolate pores exhibit strong preferred orientation coinciding with the direction of fibers while the oblate pores are randomly oriented. Note that the information on pores' geometry and orientation distribution can be readily utilized to perform micromechanical modeling of the material, the appropriate approaches are presented in [23–25,27].

6. Conclusions

A methodology for microstructure characterization of C/C composites with arbitrary fibers distribution is proposed and applied to composites with two different preforms: random felt and a 2D planar preform.

(i) For composites manufactured from both preforms, dependence of density, porosity, coating thickness and texture on the infiltration time was investigated. It was shown that, as expected, increase in infiltration time results in the decrease of porosity. Comparison of the porosity measured using water immersion (open porosity) and image analysis (total porosity) shows that difference in the obtained results is insignificant.

(ii) A methodology for fiber orientation segmentation from the μCT images of carbon fiber preforms was developed. Using that procedure, 100 different local fiber directions were resolved. The orientation distribution functions for different layers of the composite with 2D preform were extracted and visualized.

(iii) The μCT studies of the infiltrated composites were conducted and pores with irregular shapes were identified. A methodology of pore approximations by ellipsoids using principal component analysis (described in [46]) was applied to the material based on the 2D preform. The pore half-axes aspect ratios, volume and orientation distribution functions were estimated.

(iv) It was shown that the distance between fibers in the preform vary. The fibers can be differentiated into the bundles and single fibers. There is sufficient spacing between single fibers and the rest of the preform so that more PyC can deposit on single fibers during CVI resulting in thicker coating. This results in thick PyC coating around these fibers. The fibers in the bundles are close to each other and spacing between them is limited. For this reason, the growth of PyC coating continues only until this space is filled, so that the fibers in bundles have thinner coating.

(v) A methodology for numerical simulations of the growth of coating on fibers, based on the processing of cross-section images and estimation of the fiber positions, was proposed. Using this methodology, the local microstructure around single fibers and fiber bundles can be quantitatively distinguished.

The above methodologies provide an accurate description of the microstructure of C/Cs with arbitrary fiber distributions which are applicable to different types of preform architecture. The results of microstructure characterization are presented in the form of tables; the orientation distribution functions are also tabulated. Such representation is very convenient for utilization as an input for development of virtual material models and simulation of its mechanical behavior.

Acknowledgements

The authors thank Dr. B. Reznik for light microscopic images. We gratefully thank the KIT for the financial support as part of the feasibility study of young scientists (FYS) – ACTAMI. The financial support of the DFG (NSF-DFG Project: ‘‘Materials World Network: Multi-Scale Study of Chemical Vapor Infiltrated C/C Composites’’, the DFG Heisenberg fellowship PI 785) is gratefully acknowledged.

References

[1] Schwartz MM. New materials, processes, and methods technology. CRC Press, Tailor and Francis; 2006.
[2] Delhaes P. Fibers and composites. Taylor and Francis; 2003.
[3] Benzinger W, Hüttinger KJ. Chemistry and kinetics of chemical vapor infiltration of pyrocarbon-V. Infiltration of carbon fiber felt. Carbon 1999;37:941–6.
[4] Benzinger W, Hüttinger KJ. Chemistry and kinetics of chemical vapor infiltration of pyrocarbon-VI. Mechanical and structural properties of infiltrated carbon fiber felt. Carbon 1999;37:1311–22.
[5] Reznik B, Hüttinger KJ. Micro- and nanostructure of the carbon matrix of infiltrated carbon fiber felts. Carbon 2001;39:215–29.
[6] Guellali M, Oberacker R, Hoffmann MJ. Influence of heat treatment on microstructure and mechanical properties of CVI–CFC composites with medium and highly textured pyrocarbon matrices. Compos Sci Technol 2008;68(5):1115–21.
[7] Gross TS, Timoshchuk N, Tsukrov I, Piat R, Reznik B. On the ability of nanoindentation to measure anisotropic elastic constants of pyrolytic carbon. Z Angew Math Mech 2012(1–12). doi:10.1002/zamm.201100128.
[8] Piat R, Reznik B, Schnack E, Gerthsen D. Modeling the effect of microstructure on the elastic properties of pyrolytic carbon. Carbon 2003;41(9):1858–62.
[9] Peebles LH. Carbon fibers: formation, structure, and properties. Boca Raton: CRC Press; 1994.
[10] Tzeng SS, Pan JN. Densification of two-dimensional carbon/carbon composites by pitch impregnation. Mat Sci Eng 2001(316a):127–34.
[11] Wu ZJ, Brown D, Davies JM. An analytical modelling technique for predicting the stiffness of 3-D orthotropic laminated fabric composites. Compos Struct 2002;56:407–12.
[12] Hatta H, Goto K, Ikegaki S, Kawahara I, Aly-Hassan M, Hamada H. Tensile strength and fiber/matrix interfacial properties of 2D- and 3D-carbon/carbon composites. J Eur Ceram Soc 2005;25:535–42.
[13] Aly-Hassan M, Hatta H, Wakayama S, Watanabe M, Miyagawa K. Comparison of 2D and 3D carbon/carbon composites with respect to damage and fracture resistance. Carbon 2003;41:1069–78.
[14] Hatta H, Suzuki K, Shigei T, Somiya T, Sawada Y. Strength improvement by densification of C/C composites. Carbon 2001;39:83–90.
[15] Hatta H, Goto K, Aoki T. Strengths of C/C composites under tensile, shear, and compressive loading: role of interfacial shear strength. Compos Sci Technol 2005;65:2550–62.
[16] Casal E, Granda M, Bermejo J, Bonhomme J, Menéndez R. Influence of porosity on the apparent interlaminar shear strength of pitch-based unidirectional C–C composites. Carbon 2001;39:73–82.
[17] Vorel J, Sýkora J, Šejnoha M. Two step homogenization of effective thermal conductivity for macroscopically orthotropic C/C composites. Bull Appl Mech 2008;4(14):48–53.
[18] Mlekusch B. Fibre orientation in short-fibre-reinforced thermoplastics. II. Quantitative measurements by image analysis. Compos Sci Technol 1999;59:547–60.
[19] Blanc R, Germain Ch, Da Costa GP, Baylou P, Cataldi M. Fibre orientation measurements in composite materials. Composites A 2006;37:197–206.
[20] Bernasconi A, Cosmi F, Dreossi D. Local anisotropy analysis of injection moulded fibre reinforced polymer composites. Compos Sci Technol 2008;68:2574–81.
[21] Cosmi F, Bernasconi A, Sodini N. Phase contrast micro-tomography and morphological analysis of a short carbon fibre reinforced polyamide. Compos Sci Technol 2001;71(1):23–30.
[22] Requena G, Fiedler G, Seiser B, Degischer P, Michiel MD, Buslaps T. 3D-Quantification of the distribution of continuous fibers in unidirectionally reinforced composites. Composites: Part A 2009;40(2):152–63.
[23] Tsukrov I, Piat R, Novak J, Schnack E. Micromechanical modeling of porous carbon/carbon composites densified by chemical vapor infiltration. Mech Adv Mater Struct 2005;12:43–54.
[24] Piat R, Mladenov N, Tsukrov I, Verijenko V, Guellali M, Schnack E, et al. Material modeling of the CVI-infiltrated C-felt. I. Basic formulae, theory and numerical experiments. Compos Sci Technol 2006;66:2997–3003.
[25] Piat R, Mladenov N, Tsukrov I, Guellali M, Ermel R, Beck T, et al. Material modeling of the CVI-infiltrated C-felt. II. Statistical study of the microstructure, numerical analysis and experimental validation. Compos Sci Technol 2006;66:2769–75.
[26] Gebert J-M, Wanner A, Piat R, Guichard M, Rieck S, Paluszynski B, et al. Application of the micro-computed tomography for analyses of the mechanical behavior of brittle porous materials. Mech Adv Mat Struct 2008;15:467–73.
[27] Drach B, Tsukrov I, Gross T, Dietrich S, Weidenmann K, Piat R, et al. Numerical modeling of carbon/carbon composites with nanotextured matrix and 3D pores of irregular shapes. J Solids Struct 2011;48(18):2447–57.
[28] Reznik B, Gerthsen D, Zhang W, Hüttinger KJ. Texture changes in the matrix of an infiltrated carbon fiber felt studied by polarized light microscopy and selected area electron diffraction. Carbon 2003;41(2):376–80.
[29] Chen T, Reznik B, Gerthsen D, Zhang W, Hüttinger KJ. Microscopical study of carbon/carbon composites obtained by chemical vapor infiltration of 0°/0°/90°/90° carbon fiber preforms. Carbon 2005;43:3088–98.

[30] Li A, Zhang S, Reznik R, Lichtenberg S, Schoch G, Deutschmann O. Chemistry and kinetics of chemical vapor deposition of pyrolytic carbon from ethanol. Proceed Combust Inst 2001;33:1843–50.
[31] Reznik B, Gerthsen D. Microscopic study of failure mechanisms in infiltrated carbon fiber felts. Carbon 2003;11(1):57–69.
[32] Gebert J-M. Intrinsische Risse und Poren in Kohlenstoff Verbundwerkstoffen. Werkstoffwissenschaft und Werkstofftechnik NR.068. Aachen: Shaker; 2011.
[33] Golecki I. Industrial carbon chemical vapour infiltration (CVI) processes. World Carbon Fiber Compos, vol. 2. New York: Taylor and Francis; 2003.
[34] Zhang WG, Hüttinger KJ. Chemical vapor infiltration of carbon fibre felt: optimization of densification and carbon microstructure. Carbon 2002;40:2529–45.
[35] Zhang WG, Hüttinger KJ. Densification of a 2D carbon fiber preform by isothermal, isobaric CVI: kinetics and carbon microstructure. Carbon 2003;41:2325–37.
[36] Paris O, Peterlik H, Loidl D, Rau C, Weitkamp T. Microcracks in carbon/carbon composites: a microtomography investigation using synchrotron radiation. MRS Proc 678 2001;1(1):EE3.8.1–.6.
[37] Manniesing R, Viergever M, Niessen W. Vessel enhancing diffusion: a scale space representation of vessel structures. Med Image Anal 2006;10(6):815–25.
[38] Otsu N. A threshold selection method from gray-level histograms. Automatica 1975;11:285–96.
[39] Manniesing R, Viergever M, Niessen W. Vessel enhancing diffusion. Insight J 2009;1(1).
[40] Hale D. Recursive Gaussian filters. Center for wave phenomena/Colorado School of Mines, CWP-546. <http://www.cwp.mines.edu/Meetings/Project06/cwp546.pdf>; 2011.
[41] Advani SG, Tucker III CL. A tensor description of fiber orientation in short fibre composites. In: Proc 43rd Ann Tech Conf, SPE; 1985. 1113–118.
[42] Leopardi P. A partition of the unit sphere into regions of equal area and small diameter. Electron Trans Numer Anal 2006;25:309–27.
[43] Morgan P. Carbon fibers and their composites. Boca Raton: Taylor and Francis; 2005.
[44] Gebert J-M, Reznik B, Piat R, Viering B, Weidenmann K, Wanner A, et al. Elastic constants of high-texture pyrolytic carbon measured by ultrasound phase spectroscopy. Carbon 2010;48(12):3647–50.
[45] Dietrich S. Composight Project 2010. Image analysis software based on ITK/VTK. <http://www.sourceforge.net/projects/composight/>.
[46] Fukunaga K. Introduction to statistical pattern recognition. Academic Press; 1990.
[47] Kailath T. The divergence and Bhattacharyya distance measures in signal selection. Trans Commun Technol 1967;15(1):52–60.
[48] Drach B, Drach A, Tsukrov I. Characterization and statistical modeling of irregular porosity in carbon/carbon composites based on X-ray microtomography data. Z Angew Math Mech 2012(1–21). http://dx.doi.org/10.1002/zamm.201100190.